Energy Equip. Sys./ Vol. 11/No. 4/December 2023/ 387-399

ENERGY EQUIPSYS

Energy Equipment and Systems
http://energyequipsys.ut.ac.ir
www.energyequipsys.com

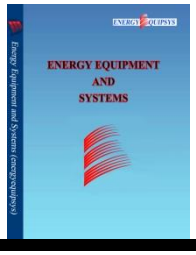

Aerodynamic design of horizontal axis wind turbine using different airfoils

Authors

Rahmat Allah Mirzaei[a]
Mojtaba Mirhosseini [a*]
Meisam Farajollahi[a]

[a] School of Advanced Technologies, Iran University of Science and Technology, Tehran, Iran

Article history:

Received : 21 March 2023
Accepted : 8 October 2023

ABSTRACT

The blade element momentum (BEM) theory has been employed to examine the aerodynamic parameters such as lift, drag, and thrust coefficient. Tip loss factor is one of the most important parameters to improve BEM theory. Glauert and Prantl represented different expressions for tip loss factor which have been used commonly in the literature. However, the measurements and theoretical analyses show that existing tip loss factors are inconsistent and fail to predict correctly the physical behavior of the blade tip. A new tip loss factor has been proposed by Shen that remedies the inconsistency. In this study, Shen's formula as the newest tip loss factor has been utilized to analyze thirteen different airfoil performances. The results indicate that the blade with the RISØ-A1-24 airfoil has the shortest chord length, approximately 1.8 meters, which is considered a significant advantage due to reduced material weight and construction costs. Moreover, the RISØ-A1-24 and FFA-W3-211 Free Transition airfoils are the most effective in terms of power generation, as their total power coefficient values versus tip speed ratio changes are higher compared to other airfoils. Additionally, airfoils such as FFA-W3-241 and S814, which reach their maximum power coefficient at lower tip speed ratios, are suitable for areas with lower average wind speeds.

Keywords: Wind Energy, Horizontal Axis Wind Turbine (HAWT), BEM Method, Aerodynamic Performance, Power Coefficient, Tip Loss Factor.

1. Introduction

Traditional power generation sources contribute significantly to pollution, necessitating further research into pollution optimization and control. This challenge has prompted international environmental and energy production organizations to explore new renewable energy resources (1). Among various renewable energy technologies, wind turbines have consistently been one of the fastest-growing. Wind turbines are undoubtedly the most critical component of wind energy systems (2). They generate energy without pollution, have short manufacturing periods, and low operating costs, which attract increasing attention (3). Wind turbines are designed to convert wind kinetic energy into usable electrical energy (2).

There are two primary categories of wind turbines based on rotor axis design: Vertical

* Corresponding author: Mojtaba Mirhosseini
School of Advanced Technologies, Iran University of Science and Technology, Tehran, Iran
Email: momi@iust.ac.ir

Axis Wind Turbines (VAWTs), where blades rotate on a vertical axis, and Horizontal Axis Wind Turbines (HAWTs), where blades rotate on a horizontal axis, nearly parallel to the wind flow. Most wind turbines produced are horizontal-axis types due to their high power coefficient (4). Accurate analysis and design of wind turbine blade aerodynamics and shape are crucial, as they extract kinetic energy from the wind and are considered one of the most important elements of wind turbines (5).

Computational Fluid Dynamics (CFD) simulations have been used in (6) to analyze the aerodynamic characteristics of the blade with different turbulence models for the NREL Phase VI wind turbine model. In (7), CFD simulation was applied to investigate the impact of turbulent wind and shear wind on floating offshore wind turbines. The power performance of wind turbines, turbine wake, and blade aerodynamics have been studied to determine the turbulence model accuracy of the CFD method for VAWTs. Additionally, CFD simulations have been employed to improve the performance of an integrated HAWT and VAWT for a specific site. Gracia-Ribeiro et al. (8) used CFD simulations to acquire the impacts by solving Reynolds-Averaged Navier-Stokes equations using a turbulence model. Pichandi et al. (9) used CFD to improve the performance of a horizontal and vertical axis wind turbine. Kuo et al. (10) used a mixed-integer programming technique with a CFD wake model to optimize wind farm in complex terrain. Hamid Arastoopour and Aiden Cohan (11) investigated the impact of rain on horizontal axis wind turbine performance. CFD simulations offer a precise but complex method for analyzing aerodynamic forces affecting the rotor, making it a time-consuming analysis that requires advanced technology systems (12).

Another method for analyzing HAWT wind turbine aerodynamic performance is the Blade Element Momentum (BEM) theory, which combines blade element theory and momentum theory (13). Unlike the CFD simulation method, BEM theory is a simple yet applicable method widely used in the wind industry (14). Several researchers have employed the BEM theory method to analyze wind turbine performance in recent years. For instance, in (15), the BEM code was used to predict the performance of a HAWT for winds typical of an urban area over a full year of operation. Echjijem and Djebli (16) also utilized the BEM method for HAWT blade design, considering the corrections of axial and tangential induction factors. They conducted BEM theory for NACA airfoil. Moreover, El-Shahat et al. (17) employed a modified BEM method coupled with linear and nonlinear wave theories to quantify the dynamic forces of a tidal stream turbine. Sang et al. (18) used a modified BEM method to simulate the aerodynamic forces and load along the blade for wind turbines. Laalej et al. (19) combined the BEM method with two-dimensional CFD simulations to predict the power of wind turbines and analyze the aerodynamic loads on the rotor blades. Vaz et al. (13) introduced a mathematical method based on BEM theory to design the horizontal axis wind turbine, considering the wake impact on the rotor plane in a general form. Wang et al. (20) used BEM theory and time-domain simulations to investigate the nonlinear aero-elastic response of a long flexible blade for a horizontal axis wind turbine. The aerodynamic performance of the rotor blades under various winds had been compared as well.

Several methods have been introduced to enhance the BEM theory performance in the last decades. The tip loss factor is one of the suggested methods represented by Prandtl (21). The tip loss factor results from the air pressure difference between the upward and downward surfaces of the profile, which causes a reduction in power produced by the wind turbine. Afterward, Glauert (22) suggested the most favored expression for the tip loss factor. Almost all of the studies in the literature have used Glauert and Prandtl tip loss factors in BEM theory. The comparison of measurements and theoretical analysis shows that existing tip loss correction models are inconsistent and fail to predict correctly the physical behavior in the proximity of the tip. Hence, in this study, a novel tip loss factor model proposed by Shen et al. (23) is used in the BEM code, which results in much better predictions of loading in the tip area.

Selecting the appropriate airfoil for blade design has a significant impact on the aerodynamic performance of wind turbines, as

the airfoil type is the main parameter determining the blade geometry. Therefore, choosing an appropriate airfoil with minimal local chord length and twist angle, and a high lift-to-drag ratio, improves the rotor's aerodynamic performance (24). Despite numerous studies on wind turbine design, there is a lack of comprehensive literature comparing different airfoils to find the optimal airfoil in various families. This article aims to investigate some different airfoils for use along the blade to fill this gap to some extent. Therefore, the BEM method has been used to analyze the aerodynamic performance of a 200 kW horizontal axis wind turbine with different airfoils. Thirteen airfoil types, including RISØ-A1-18, RISØ-A1-21, RISØ-A1-24, FFA-W3-211 Fixed Transition, FFA-W3-211 Free Transition, FFA-W3-241, FFA-W-301, S809, S814, FX66-S196-V1, DU 91-W2-250, DU-W-210, and A-Airfoil, have been investigated in this article.

Nomenclature

ρ	Air density
R	The radius of the wind turbine
B	Number of blades
a	Axial induction factor
b	Angular induction factor
α	Angle of attack
θ_p	Pitch angle
θ_T	Twist angle
P	The power generated by wind turbine
V_0	Free flow wind velocity
V_t	Tangential velocity in the far wake
V_n	Normal velocity in the far wake
U_n	The normal velocity of the rotor
U_0	Longitudinal velocity for upstream
U_t	Tangential velocity of the rotor
r	The local radius along the blade
σ	Solidity of rotor
ϕ	Inflow angle
Ω	Angular velocity of the rotor
M	Torque
T	Thrust
D	Drag force
L	Lift force
C_l	Lift coefficient
C_d	Drag coefficient
C_p	Power coefficient
C_t	Thrust coefficient
F	Tip loss factor
λ	Tip speed ratio
η	Electrical-mechanical efficiency

2. BEM theory

As mentioned above, the BEM method was first introduced by Glauert [22] to calculate the aerodynamic forces on wind turbines. Blade element theory was combined with momentum theory to form the BEM method. In this approach, the blade is divided into several independent sections, and the aerodynamic loads affecting each section are computed on a two-dimensional airfoil subjected to flow conditions. Figure (1) illustrates the velocities and forces impacting a cross-section of a rotor blade.

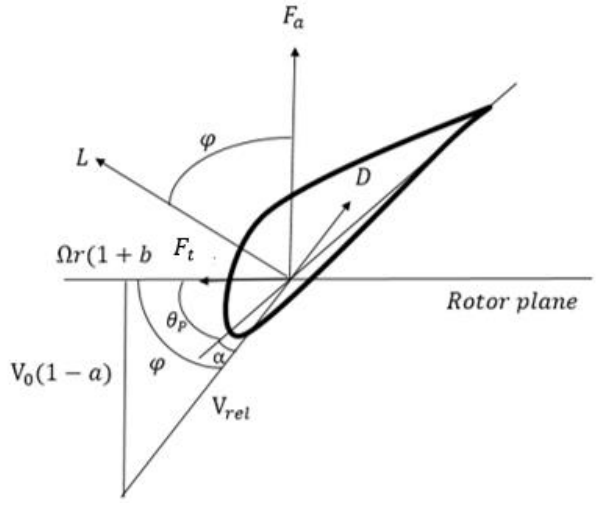

Fig. 1. velocities and forces related to cross-sectional airfoil element

V_o and Ω are the free flow wind velocity and the angular velocity of rotor, respectively. The axial and angular induction factors are denoted by a and b, respectively. α is the angle of attack, θ_P is pitch angle, and φ is the angle of the relative wind. Additionally, the lift and drag forces are L and D, respectively which are defined as

$$L = \frac{1}{2}\rho V_0^2 A C_l \tag{1}$$

and

$$D = \frac{1}{2}\rho V_0^2 A C_d \tag{2}$$

where A is the area of the rotor, ρ is the air density, and C_l and C_d are lift and drag coefficients, respectively. The axial part (F_a) creates the thrust of the rotor, while the tangential component (F_t) is the major reason for rotor torque. By applying mass and angular momentum equations for each section of the blade (dr), the thrust and torque for the rotor can be calculated, respectively, as

$$dT = \frac{1}{2}\rho B V_0^2 \frac{(1-a)^2}{sin^2\phi} c\left(C_l cos\phi + C_d sin\phi\right) dr \tag{3}$$

and

$$dM = \frac{1}{2}\rho B V_0 \frac{(1-a)(1+b)}{sin\phi cos\phi} c\left(C_l cos\phi - C_d sin\phi\right) r dr \tag{4}$$

where B is the number of blades, r is the local radius. In the second part of the BEM method, momentum theory had been applied for annular elements, hence thrust and torque for each part are defined, respectively, as

$$dT = 4\pi\rho B V_0^2 a(1-a) r dr \tag{5}$$

and

$$dM = 4\pi\rho B V_0 \Omega b(1-a) r^3 dr \tag{6}$$

Finally, the axial and the angular induction factors can be calculated by equating (3) with (5), and (4) with (6), which gives

$$b = \frac{1-3a}{4a-1} \tag{7}$$

and

$$b = \frac{1-3a}{4a-1} \tag{8}$$

where the solidity of the rotor is given by

$$\sigma = \frac{Bc}{2\pi r} \tag{9}$$

In fact, BEM theory is based on assumptions that do not fully account for the actual flow characteristics around the blade. Prandtl (Manwell et al [25]) introduced a model to account for the effect of tip flow from the lower-pressure downward surface to the higher-pressure upward surface, resulting in a reduction of lift and, hence, power generation at the tip area. This phenomenon is called the tip loss factor (F), as it changes the tip direction, leading to aerodynamic loss. Accounting for the tip loss factor is crucial for wind turbines with a low number of blades. Glauert [22] later defined the implementation of the tip loss factor in blade element theory. In this article, the aerodynamic performance of the rotor using BEM theory is analyzed with the tip loss correction proposed by Shen [20]. Shen suggested a new semi-empirical (F), incorporating another correction to the 2D airfoil data in the tip area. The proposed F is similar to the one presented by Glauert [22] and is defined as

$$F_{Shen} = \frac{2}{\pi}\text{acosexp}\left[\left(-g(\lambda)\frac{B}{2}\frac{R-r}{Rsin\Phi_R}\right)\right] \tag{10}$$

where g is a coefficient which required to be determined. Normally, g depends on λ, chord length, pitch angle distribution, etc. For simplicity, this correction is deemed to be relying on the B and λ as

$$g(\lambda) = \exp\left[-c_1\left(B\lambda - c_2\right)\right] \tag{11}$$

From experimental data, c_1 and c_2 coefficients have been determined. Two different tip speed ratios are required since there are only two coefficients. The NREL data at a wind speed of 10 $^{m}/_{s}$, comparable to λ = 3.79, and the Swedish WG 500 rotor at a $\lambda = 14$ was applied to cover a broad spectrum of tip speed ratio. A simple curve fit from a comparison between calculated and measured distributions of the normal force in the tip region showed that $c_1 \approx 0.125$ and $c_2 = 21$. Besides, the g function has a shift of 0.1 to prevent deterioration when the tip speed ratio tends to infinity. Hence, the ultimate coefficient (g) function is written as

$$g(\lambda) = \exp\left[-0.125\left(B\lambda - 21\right)\right] + 0.1 \tag{12}$$

BEM method equations will be changed by applying F as

$$dT = 4F\pi\rho BV_0^2 a(1-a)rdr \tag{13}$$

$$dM = 4F\pi\rho BV_0\Omega b(1-a)r^3 dr \tag{14}$$

and

$$C_t = 4aF(1-a) = \frac{\sigma(1-a)^2(C_l cos\phi + C_d sin\phi)}{sin^2\phi} \tag{15}$$

According to Manwell et al [25], a is defined as

$$a = \frac{1}{\left(1+\frac{4Fsin^2\phi}{\sigma C_l cos\phi}\right)} \tag{16}$$

when $C_t < 0.96$, unless it is defined as

$$a = \left(\frac{1}{F}\right)\left[0.143+\sqrt{0.0203-0.6427(0.889-C_t)}\right] \tag{17}$$

Furthermore, the angular induction factor defines as

$$b = \frac{1}{\frac{4Fcos\phi}{\sigma C_l}-1} \tag{18}$$

Finally, the total power coefficient will be calculated by an iterative method mentioned in Manwell et al [25] as

$$C_{ptot} = \frac{8}{\lambda n}\sum_{i=1}^{n} F_i sin^2\phi_i (cos\phi_i - \lambda_{ri} sin\phi_i)(sin\phi_i - \lambda_{ri} cos\phi_i)\left[1-\left(\frac{C_d}{C_l}\right)cot\phi_i\right]\lambda_{ri}^{\ 2} \tag{19}$$

where λ_r is the local tip speed ratio defined as

$$\lambda_r = \frac{r\Omega}{V_0}$$

3. Wind turbine design

The general approach to rotor design begins by defining various rotor parameters and airfoil types. The optimal blade shape is determined by considering wake rotation, and the blade's initial shape is established. The final shape and performance of the blade are determined through iterative evaluations of tip losses, drag, and manufacturability. To determine the fundamental parameters of the rotor, it is necessary to establish the power generated by the wind (P) at a specific wind velocity (U). Thus, the rotor radius (R) can be calculated using

$$P = \frac{1}{2}C_p\eta\rho\pi R^2 U^3 \tag{20}$$

In this equation, η represents the electromechanical efficiency [24], which is considered 0.8 in this study. The wind velocity (U) is considered to be 8 m/s. In the next step, the design lift, drag, and angle of attack are selected using experimental curves for local aerodynamic characteristics of the airfoil, ensuring that the lift-to-drag ratio (LDR) remains at its highest value. The experimental results for the $RISØ-A1$ family are provided in [27].

Griffiths [28] demonstrated that LDR significantly impacts the power coefficient, as a high lift coefficient directly enhances power output. Once the airfoil's aerodynamic efficiency has been determined, the maximum power coefficient ($C_{p,max}$) for an optimal tip speed ratio can be calculated using

$$C_{pmax} = \left(\frac{16}{27}\right)\lambda\left[\lambda+\frac{1.32+\left[\frac{\lambda-8}{20}\right]^2}{B^{2/3}}\right]^{-1} - \frac{(0.57)\lambda^2}{\frac{C_l}{C_d}\left[\lambda+\frac{2}{2B}\right]} \tag{21}$$

C_{pmax} is used for calculating the rotor swept area (Eq. (20)) in the primary stages of design. In this study, the number of blades is set to three, as wind turbines with fewer than three blades present various construction challenges that must be considered in the hub design [27]. Next, the blade geometry with a midpoint radius for each section of the blade can be obtained using optimal rotor theory, as follows:

$$\lambda_{r,i} = \lambda_{opt}\left(r_i/R\right) \tag{22}$$

$$\varphi_i = \frac{2}{3}tan^{-1}\left(\frac{1}{\lambda_{r,i}}\right) \tag{23}$$

$$c_i = \frac{8\pi r_i}{BC_{l,dsign}}(1-cos\varphi_i) \tag{24}$$

$$\theta_{T,i} = \theta_{p,i} - \theta_{p,0} \tag{25}$$

and

$$\theta_{p,i} = \varphi_i - \alpha_{design} \tag{26}$$

Table 1 lists important variable parameters in the aerodynamic design of the rotor for different chosen airfoils, including the $RISØ-A1$ family series, FFA-W3-211 Fixed Transition, FFA-W3-211 Free Transition, FFA-W3-241, FFA-W3-301, S809, S814, FX66-S196-V1, DU 91-W2-250, DU-W-210, and A-Airfoil.

Table 1. Important variable parameters in aerodynamic design for different airfoils

Selected airfoils	Aerodynamic design parameters			
	α_{design}	$\frac{C_{l,design}}{C_{d,design}}$	$C_{p,max}$	λ_{opt}
$\boldsymbol{RIS\emptyset - A1 - 18}$	7.9	79.53	0.50	7.50
$\boldsymbol{RIS\emptyset - A1 - 21}$	8.1	72.34	0.50	8.50
$\boldsymbol{RIS\emptyset - A1 - 24}$	10.4	56.77	0.5125	8.93
FFA-W3-211 Fixed Transition	6.2	54.15	0.4819	5.90
FFA-W3-211 Free Transition	6.7	181.44	0.5260	9.60
FFA-W3-241	11.7	45.08	0.4732	5.80
FFA-W3-301	7.4	29.98	0.4364	5.50
S809	6.3	93.64	0.50	7.10
S814	7.6	70.28	0.4881	6.10
FX66-S196-V1	8.7	127.08	0.5143	8.30
DU 91-W2-250	9.2	104.83	0.5066	7.70
DU-93-W-210	8.1	99.05	0.5143	8.30
A-Airfoil	7.9	62.82	0.4819	6.00

4. Result and discussion

As previously mentioned, selecting the appropriate airfoil has a significant impact on the aerodynamic performance of the rotor and the blade's shape. Various airfoil types are currently used in wind turbine manufacturing. In this article, thirteen different airfoils, commonly employed in the wind turbine industry, have been economically and aerodynamically investigated for a 200 kW horizontal-axis wind turbine. Initially, the optimal rotor theory was utilized to determine the blade's local geometry. Then, the BEM theory method was employed to analyze rotor performance. In Fig. (2), chord length distributions along the blade are shown for different airfoils. Two important observations can be made here. First, for all studied airfoils, the local chord length is larger at the root area than at the tip area. Second, among all other airfoils, the blade with FFA-W3-301 and S809 airfoils has the largest chord length (approximately 5.1 and 4.7 meters, respectively) at the interior parts of the blade due to their lower design lift coefficient among all chosen airfoils (according to Table (1)). Conversely, the blade with RISØ-A1-24 airfoil has the lowest chord length, about 1.79 meters at the root regions, since it has the highest C_(l,design), which is considered a significant advantage due to reduced material weights and construction costs.

Figure (3) illustrates that the local twist angle for different airfoils decreases similarly from nearly 47 degrees at the interior sections of the blade to 0 degrees at the tip region, as the blade speed increases when moving through the airflow. The twist angle reduction manner across the blade helps the angle of attack at each section to maintain at its optimal value, and consequently, the lift coefficient remains at the maximum value [29].

The angle of relative wind (φ_i) is shown in Fig. (4). It exhibits a similar reduction for various airfoils, starting from approximately 55 degrees at the root region to nearly 5 degrees at the blade tip. Furthermore, the continuous reduction in the angle of relative wind along the blade leads to optimal LDR, resulting in the optimum lift coefficient for each section along the blade. Figure (5) displays solidity across the blade for different airfoils. Solidity as a crucial design parameter, is defined as the ratio of blade area to swept area (according to Eq. (9)). The diagram reveals that all airfoils have a larger value at the root area due to the high chord length, which then decreases along the blade until it reaches zero at the blade tip. Moreover, S809 and FFA-W3-301 have the highest solidity, while $RIS\emptyset - A1 - 24$ has the lowest value for solidity in the interior part of the blade due to their chord length at the blade root.

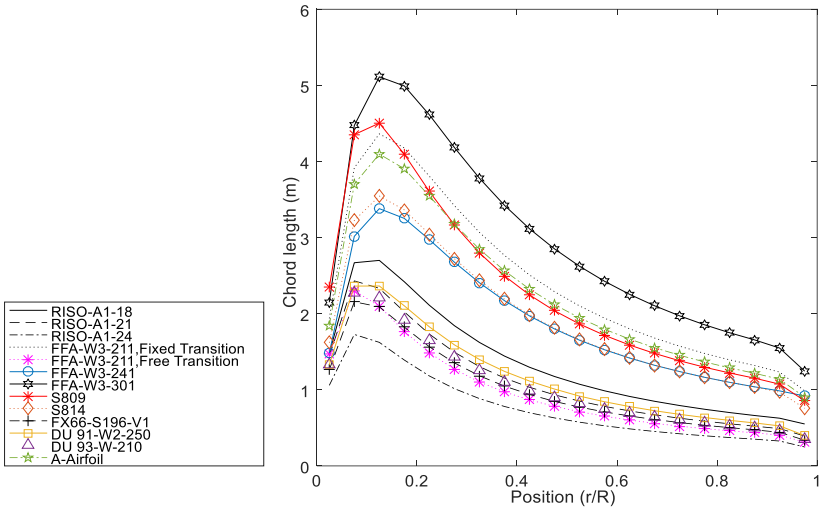

Fig. 2. Local chord length for chosen airfoils

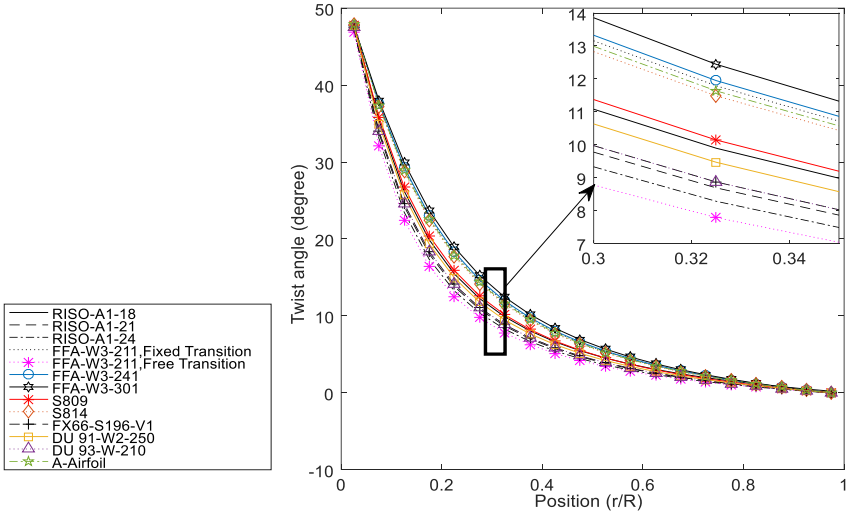

Fig. 3. Local twist angle for chosen airfoils

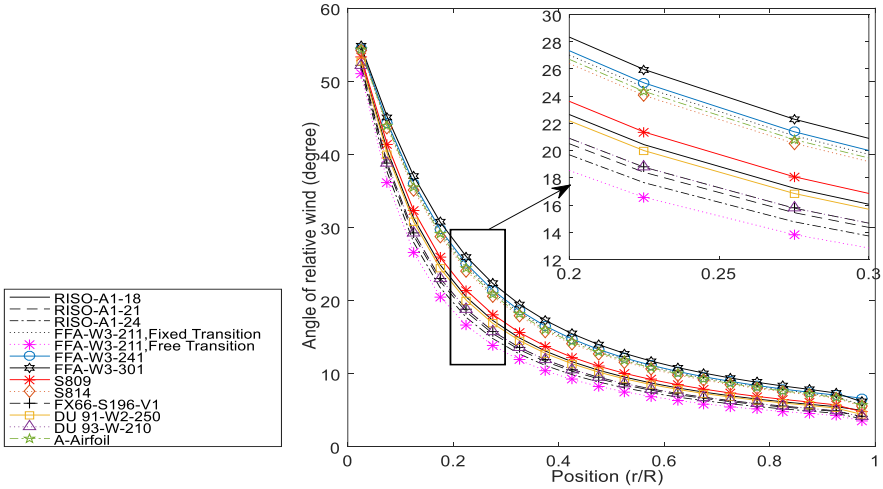

Fig. 4. Local angle of relative wind for chosen airfoils

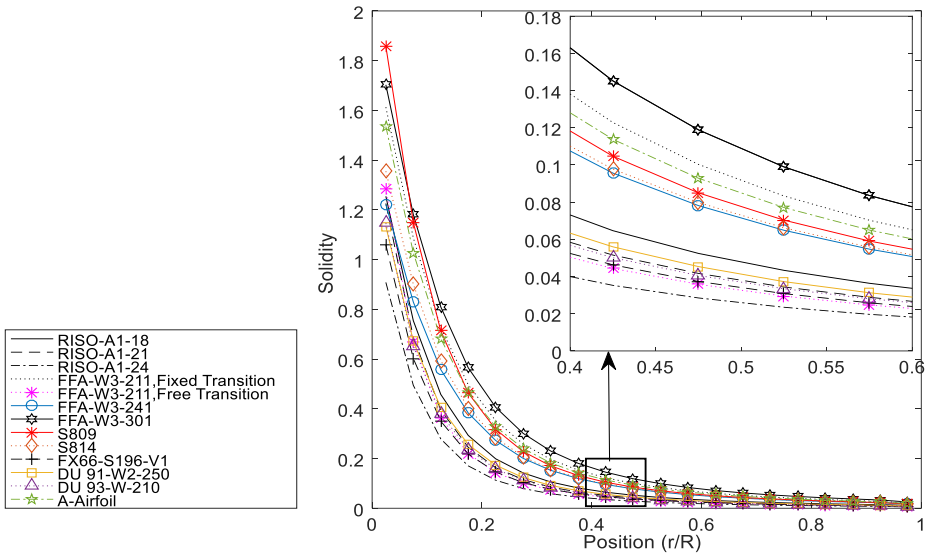

Fig. 5. Local solidity for selected airfoils

Figure (6) represents the tip loss factor, (F), for different airfoils. As previously observed in Eq. (12), the tip loss correction, as expressed by Shen, depends solely on the optimal tip speed ratio (λ_{opt}) and the number of blades. Hence, F has varying influences on airfoils with different λ_{opt}, as the number of blades remains constant in this work. As shown, FFA-W3-211 Free Transition and $RISØ-A1-24$ airfoils have the lowest tip loss values, approximately 40% and 37% respectively, while FFA-W3-301 and FFA-W3-241 airfoils have the highest tip loss values, about 1 and 4%, respectively. In Figure (7), except for a reduction at the blade tip caused by the tip loss effect, the angle of attack remains at a constant value at each section to achieve the maximum LDR and, therefore, the maximum power generation [25]. The FFA-W3-241 airfoil has the highest angle of attack, around 11.7 degrees, with a low tip loss effect due to its high design angle of attack and low optimum tip speed ratio. Next, $RISØ-A1-24$ has the highest angle of attack with a much greater tip-loss effect of about 7% at the blade tip, as this airfoil has a higher design angle of attack of approximately 10.4 degrees and a higher optimal tip speed ratio (λ_{opt} = 8.93). Finally, S809 and FFA-W3-211, Fixed Transition airfoils have the lowest angle of attack, about 6.3 degrees along the blade, due to their lower design angle of attack.

The local lift coefficient possesses a constant value for 90% of the blade length for different airfoils, as shown in Fig. (8). This constant lift coefficient results in achieving the maximum power generation of the wind turbine. The $RISØ-A1-24$ airfoil has the highest lift coefficient due to its highest design lift coefficient (according to Table (1)). However, it also has a higher design angle of attack and optimum tip speed ratio than other airfoils, which is considered a drawback because it requires a higher tip speed ratio to achieve its maximum power production.

Figure (9) displays the local drag coefficient, which is approximately constant for each element across different blades. The constant value for the local drag coefficient results from the constant angle of attack distributions along the blade, leading to optimal LDR maintenance and, consequently, maximum power production. The results indicate that the FFA-W3-301 airfoil has the highest value for the drag coefficient along the blade, equal to 0.033, leading to a lower power coefficient. On the other hand, the FFA-W3-211 Free Transition airfoil has the lowest drag coefficient ($C_d = 0.006$), resulting in a higher power coefficient than other airfoils. Figure (10) reveals that the local axial induction factor for different airfoils maintains a constant value (about 0.33) for 65% of the blade length ($0.3 < {}^{r}/_{R} < 0.9$). The axial induction factor should remain around 0.33 according to the Betz limit [21] to achieve the maximum efficiency of an aerodynamic horizontal-axis rotor. On the other hand, the maximum power coefficient

(Betz limit) occurs at an axial induction factor of 1/3. Additionally, the axial induction factor increases at the blade tip with different airfoils, as it is inversely proportional to the tip loss factor (Eq. (17)). It is clear that the FFA-W3-241 airfoil has the lowest value for the axial induction factor at the blade tip due to its lowest tip loss effect. Moreover, except for $0.2 < {}^{r}/_{R} < 0.85$ and $RISØ - A1 - 21$ airfoils, all other airfoils have nearly the same value for the axial induction factor at the tip area. In Fig. (11), thrust coefficient distributions are shown for different airfoils along the blade. The results reveal that C_t starts from 0.81 for all airfoils, then reaches a constant value ($C_t = 0.89$) at 55% along the blade, and finally decreases due to the tip loss factor impact at the tip region. A lower thrust coefficient improves blade lifespan and reduces costs. Therefore, except for $RISØ - A1 - 18$, $RISØ - A1 - 21$, and FFA-W3-241 airfoils, all other airfoils have similar values, around 0.62, for the thrust coefficient at the blade tip. Additionally, FFA-W3-241 airfoils have the highest thrust coefficient, about 0.87, at the blade tip.

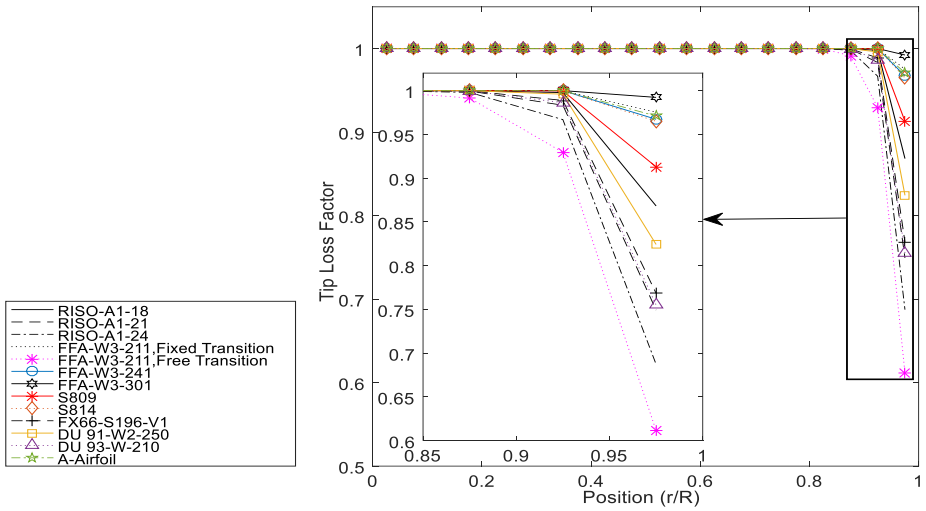

Fig. 6. Local tip loss factor for selected airfoils

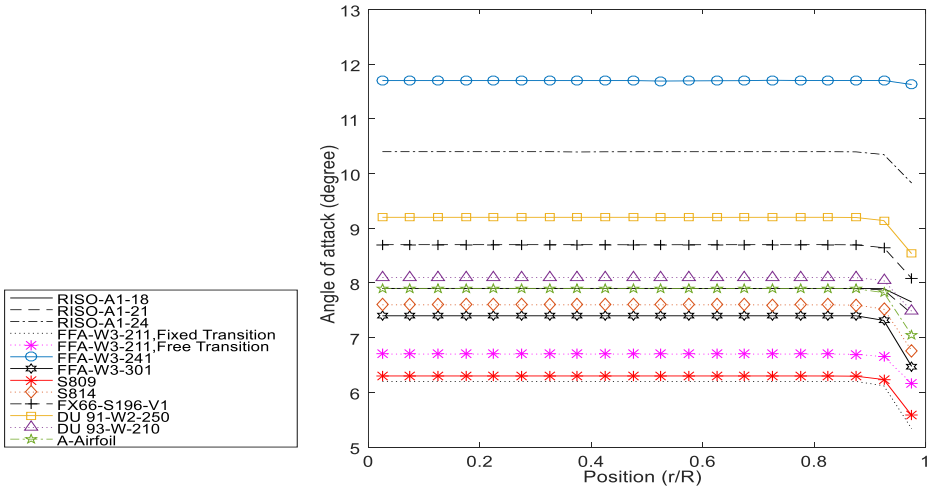

Fig. 7. Local angle of attack for selected airfoils

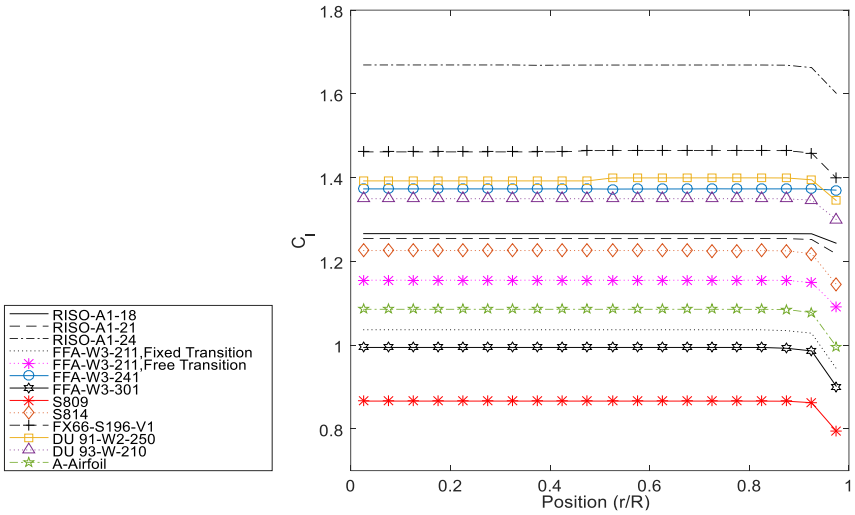

Fig. 8. Local lift coefficient for selected airfoils

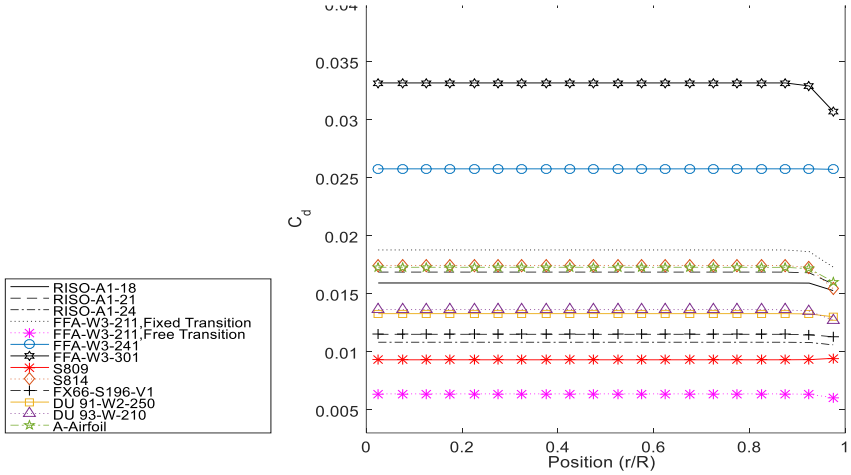

Fig. 9. Local drag coefficient for selected airfoils

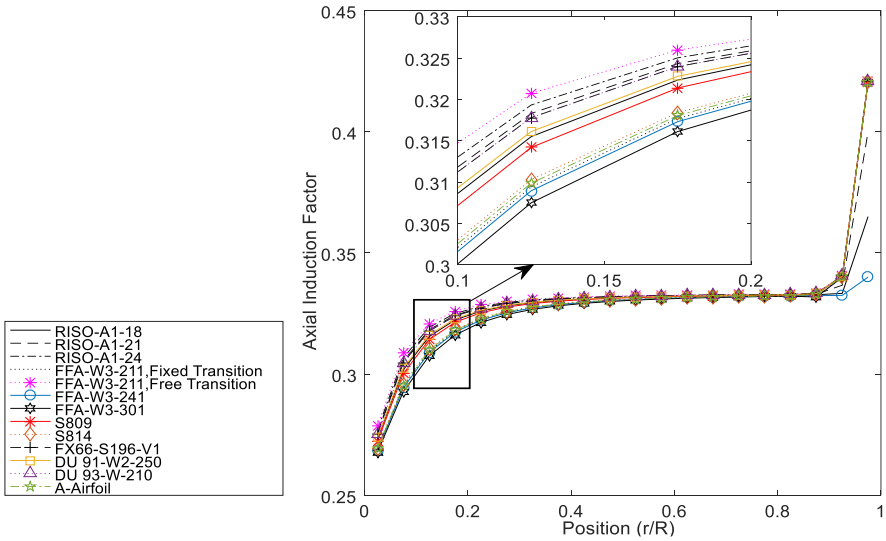

Fig. 10. Local axial induction factor for selected airfoils

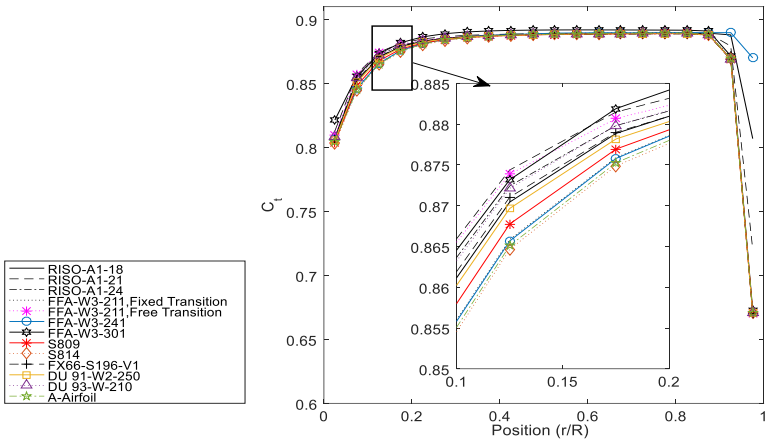

Fig. 11. Local thrust coefficient for selected airfoils

As evident from Fig. (12), the power coefficient change along the blade follows an almost linear function for nearly 90% of the blade length, except for the tip region. It is worth noting that when the root region loads are minimal, the force distributions across the blade are optimal, which is achievable by decreasing the maximum lift coefficient around the tip area. According to the diagram, different airfoils exhibit the same behavior for the local power coefficient, except for the FFA-W3-301 airfoil. This airfoil generates lower power than other airfoils at the tip area due to its much higher drag lift along the blade (see Fig. (9)). Furthermore, all different airfoils reach their maximum power coefficient at 90% of the blade length. Figure (13) displays the total power coefficient of the designed blade with different airfoils that have been investigated versus various tip speed ratios. As shown, the total $C_{p,tot}$ increases with λ increments to reach their maximum values, then begins to decrease for higher tip speed ratios. The results are entirely predictable, as each airfoil is designed at λ_{opt} to achieve $C_{p,max}$, and it is evident that other tip speed ratios lead to power coefficient reduction. The FFA-W3-301 airfoil has the lowest power coefficient among all chosen airfoils due to its highest drag coefficient. Moreover, the $C_{p,max}$ values versus tip speed ratio changes for this airfoil are much lower than those of other airfoils. Except for the FFA-W3-301 airfoil, all other airfoils have nearly the same total power coefficient at different λ_{opt}, but the RISØ-A1-24 and FFA-W3-211, Free Transition airfoils are the best selections because their $C_{p,tot}$ values versus λ changes are higher among all different airfoils. Furthermore, airfoils such as FFA-W3-241 and S814, which reach their maximum power coefficient at lower tip speed ratios, are suitable for areas with lower average wind speeds.

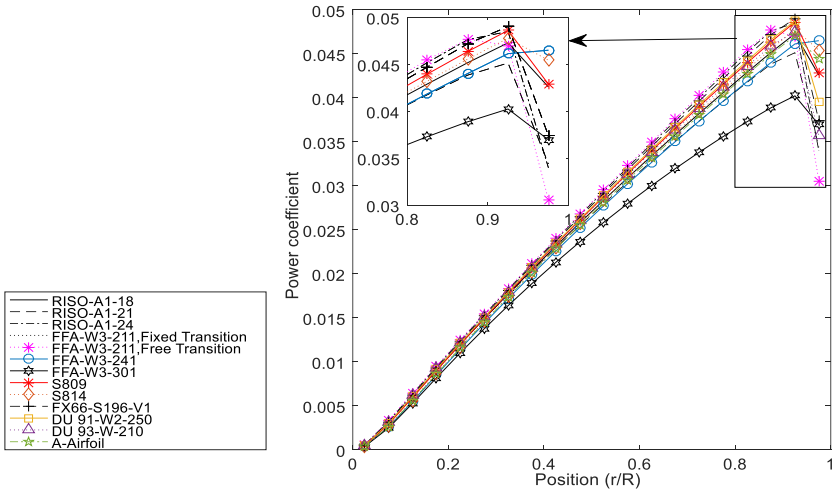

Fig. 12. Local power coefficient for selected airfoils

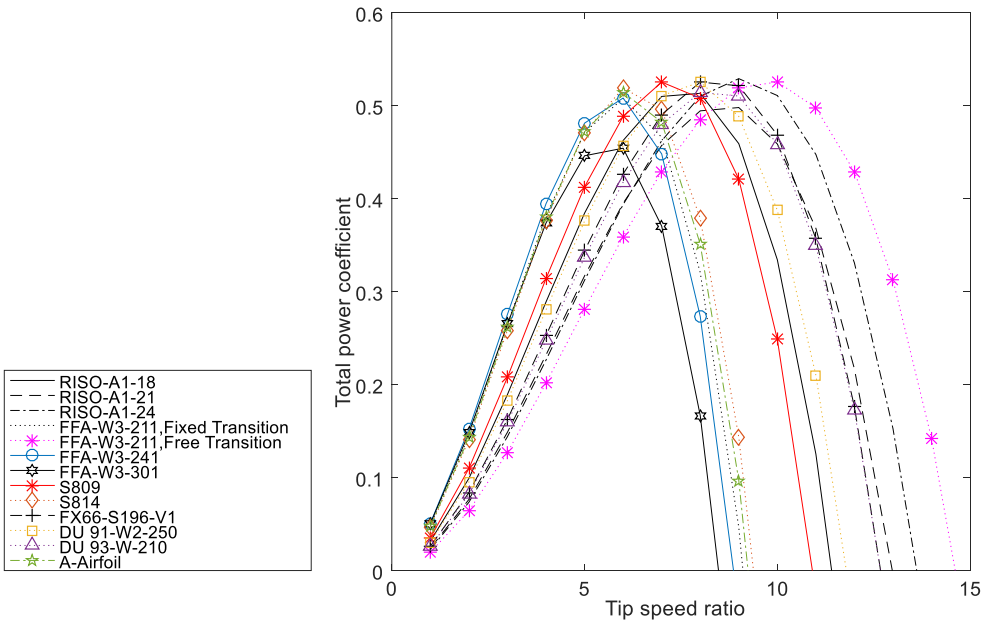

Fig. 13. total power coefficient versus different tip speed ratios for selected airfoils

5. Conclusion

In this study, thirteen various airfoils commonly used in the wind turbine industry have been investigated. The BEM theory has been employed to analyze the aerodynamic performance of the rotor. In addition, the Shen tip loss factor has been used in the BEM method, which shows better stability in analyzing the aerodynamic load at the tip area of the rotor blades than the tip loss factor models proposed by Prandtl and Glauert. The selected wind turbine is a 200 kW horizontal axis wind turbine with three blades. The results indicate that the blade with the RISØ-A1-24 airfoil has the shortest chord length of about 1.79 meters at the root regions, which is considered a significant advantage due to reduced material weight and construction costs. Moreover, the local twist angle and the angle of relative wind exhibit a similar reduction trend for all different airfoils to achieve the optimal LDR and, consequently, the optimal lift coefficient for each section along the blade. On the other hand, the diagram of the total power coefficient of the designed blade with different airfoils versus various tip speed ratios shows that $C_{p,tot}$ increases with λ increments, reaching their maximum values before decreasing for higher tip speed ratios. The FFA-W3-301 airfoil has the lowest power coefficient among all chosen airfoils due to its highest drag coefficient. Furthermore, the RISØ-A1-24 and FFA-W3-211 Free Transition airfoils are the best choices, as the $C_{p,tot}$ values for these two airfoils versus λ changes are higher among all different airfoils. Additionally, airfoils such as FFA-W3-241 and S814, which reach their maximum power coefficient at lower tip speed ratios, are suitable for areas with lower average wind speeds.

References

[1] Gu B, He M, Yang D, Yue X, Qiu F, Zhang T, et al. Wearable Janus MnO2 hybrid membranes for thermal comfort management applications. Applied Surface Science. 2020;509:145170.

[2] Hand B, Kelly G, Cashman A. Aerodynamic design and performance parameters of a lift-type vertical axis wind turbine: A comprehensive review. Renewable and Sustainable Energy Reviews. 2021;139:110699.

[3] Zhang Z, Wang H, Zhang Y, Feng W. Enhanced wind turbine maximum wind-energy capture based on the inverse-system method. Energy Reports. 2022;8:475-87.

[4] Saeidi D, Sedaghat A, Alamdari P, Alemrajabi AA. Aerodynamic design and economical evaluation of site specific small vertical axis wind turbines. Applied energy. 2013;101:765-75.

[5] Patel H, Damania S. Performance prediction of horizontal axis wind turbine blade. International journal of innovative research in science, engineering and technology. 2013;2(5):1401-6.
[6] Ji B, Zhong K, Xiong Q, Qiu P, Zhang X, Wang L. CFD simulations of aerodynamic characteristics for the three-blade NREL Phase VI wind turbine model. Energy. 2022;249:123670.
[7] Zhou Y, Xiao Q, Liu Y, Incecik A, Peyrard C, Wan D, et al. Exploring inflow wind condition on floating offshore wind turbine aerodynamic characterisation and platform motion prediction using blade resolved CFD simulation. Renewable Energy. 2022;182:1060-79.
[8] Garcia-Ribeiro D, Flores-Mezarina JA, Bravo-Mosquera PD, Cerón-Muñoz HD. Parametric CFD analysis of the taper ratio effects of a winglet on the performance of a Horizontal Axis Wind Turbine. Sustainable Energy Technologies and Assessments. 2021;47:101489.
[9] Pichandi C, Pitchandi P, Kumar S, Sudharsan NM. Improving the performance of a combined horizontal and vertical axis wind turbine for a specific terrain using CFD. Materials Today: Proceedings. 2022;62:1089-97.
[10] Kuo JY, Romero DA, Beck JC, Amon CH. Wind farm layout optimization on complex terrains–Integrating a CFD wake model with mixed-integer programming. Applied Energy. 2016;178:404-14.
[11] Arastoopour H, Cohan A. CFD simulation of the effect of rain on the performance of horizontal wind turbines. AIChE Journal. 2017;63(12):5375-83.
[12] Li Y, Castro A, Sinokrot T, Prescott W, Carrica P. Coupled multi-body dynamics and CFD for wind turbine simulation including explicit wind turbulence. Renewable Energy. 2015;76:338-61.
[13] Vaz JRP, Pinho JT, Mesquita ALA. An extension of BEM method applied to horizontal-axis wind turbine design. Renewable Energy. 2011;36(6):1734-40.
[14] DNV G, Hassan G. Tidal Bladed Theory Manual. Energy Headquarters: Arnhem, The Netherlands. 2012.
[15] Atlaschian O, Metzger M. Numerical model of vertical axis wind turbine performance in realistic gusty wind conditions. Renewable Energy. 2021;165:211-23.
[16] Echjijem I, Djebli A. Design and optimization of wind turbine with axial induction factor and tip loss corrections. Procedia Manufacturing. 2020;46:708-14.
[17] El-Shahat SA, Fu L, Li G. Linear and non-linear wave theories coupled with a modified BEM model for quantifying dynamic loads of a tidal stream turbine. Ocean Engineering. 2022;243:110334.
[18] Sang S, Wen H, Cao A, Du X, Zhu X, Shi Q, et al. Dynamic modification method for BEM of wind turbine considering the joint action of installation angle and structural pendulum motion. Ocean Engineering. 2020;215:107528.
[19] Laalej S, Bouatem A, AlMers A, El Maani R. Wind turbine performances prediction using BEM approach with Jonkman-Buhl brake state model coupled to CFD method. Materials Today: Proceedings. 2022;65:3829-38.
[20] Wang Z, Lu Z, Yi W, Hao J, Chen Y. A study of nonlinear aeroelastic response of a long flexible blade for the horizontal axis wind turbine. Ocean Engineering. 2023;279:113660.
[21] Prandtl L. Applications of modern hydrodynamics to aeronautics: US Government Printing Office; 1925.
[22] Glauert H. Airplane propellers. In: Durand WF editor. Aerodynamic theory. 1963.
[23] Shen WZ, Mikkelsen R, Sørensen JN, Bak C. Tip loss corrections for wind turbine computations. Wind Energy: An International Journal for Progress and Applications in Wind Power Conversion Technology. 2005;8(4):457-75.
[24] Sedaghat A, Mirhosseini M. Aerodynamic design of a 300 kW horizontal axis wind turbine for province of Semnan. Energy conversion and management. 2012;63:87-94.
[25] Manwell JF, McGowan JG, Rogers AL. Wind energy explained: theory, design and application: John Wiley & Sons; 2010.